DOI: 10.1002/fuce.200400073





# Multidimensional Modelling of Polymer Electrolyte Fuel Cells under a Current Density Boundary Condition

H. Meng[1], and C.-Y. Wang[1]*

[1] Electrochemical Engine Center (ECEC), and Department of Mechanical and Nuclear Engineering, The Pennsylvania State University, 338A Reber Building, University Park, PA 16802, USA

Received May 27, 2004; accepted November 15, 2004

## Abstract

A three-dimensional numerical model of the polymer electrolyte fuel cell (PEFC) is applied to study current distribution and cell performance under a current density boundary condition. Since the electronic resistance in the along-channel direction in the current collector plate is much larger than in the other two directions, i.e., 50 $m\Omega\ cm^2$ *vs.* 0.5 $m\Omega\ cm^2$, it significantly affects current flow, and current and cell voltage distributions in a PEFC. An identical polarization curve results with two different boundary conditions, constant cell voltage and constant current density, however, the current density profiles in the along-channel direction differ significantly; it is much flatter for the constant current boundary condition. Increasing the electronic conductivity of the bipolar plate diminishes the difference in the current density distribution under the two boundary conditions. The results also point out that an experimental validation of a PEFC model based on the polarization curve alone is insufficient, and that detailed current density distribution data in the along-channel direction is essential.

**Keywords:** Current Density Boundary Condition, Current Distribution, Electron Transport, Polymer Electrolyte Fuel Cell, Stoichiometry Control

## 1 Introduction

The polymer electrolyte fuel cell (PEFC) is a promising alternative power source for application to transportation because of its high efficiency, low emissions, and low noise. However, before its commercialisation, a few obstacles need to be overcome. Among them, a fundamental understanding of the design and engineering optimisation of fuel cell systems with a higher durability and lower cost is required. In recent years, numerical modelling and simulation has become an important tool for enhancing the physical understanding, and optimising the design and operation of the PEFC. Many two- and three-dimensional PEFC models have been developed for these purposes [1–12]. In these numerical models, computational fluid dynamics (CFD) methodology has been employed to integrate transport phenomena, electrochemical processes, and water/proton co-transport in the polymer electrolyte to enable multi-physics modelling and large-scale simulation.

The majority of previous multidimensional models are restricted to using constant cell voltage as the boundary condition, while fuel cell experiments are carried out predominantly under constant total current and stoichiometry control, where the reactant flow-rates vary with the applied current to maintain a true stoichiometric constant. The overriding objective of the present work is to propose an elegant method to enable multidimensional modelling of PEFCs under a current density boundary condition. This is achieved by accounting for electron transport through the electronic components of a PEFC.

In all the previous PEFC models, electron transport in the catalyst and gas diffusion layers, as well as in the current collector plate, was ignored, by assuming constant electronic phase potential in these materials. This assumption was demonstrated to be inappropriate by Meng and Wang [13], especially in the through-plane direction with contact resistances between two mating materials. Furthermore, it was shown that the lateral electronic resistance in the GDL, which depends on electronic conductivity, GDL thickness, and gas channel width, plays a critical role in determining the current

[*] *Corresponding author, cxw31@psu.edu*

distribution and cell performance. Thus, the inclusion of GDL electron transport enables the thickness and width of the GDL and width of the gas channel to be optimised for improved current distribution and cell performance.

The assumption of constant electronic phase potential could be inappropriate in the bipolar plate. The typical bipolar plate length is 100,000 μm, while its width and depth are of the order of 1,000 μm. Since the electronic conductivity of the plate is 20,000 S $m^{-1}$ for graphite-based materials [14], the electronic resistances in the lateral and through-plane directions are only 0.5 mΩ $cm^2$. The electronic resistance in the along-channel direction, however, can reach 50 mΩ $cm^2$, which could significantly affect current redistribution in the PEFC.

In this paper, a three-dimensional, isothermal, electrochemical and transport fully coupled polymer electrolyte fuel cell (PEFC) model [13] is applied to explore the effect of the electronic resistance in the along-channel direction of the bipolar plate on current distribution and cell performance under the current density boundary condition.

## 2 Numerical Model

A three-dimensional, single-phase, isothermal numerical model of polymer electrolyte fuel cells, which was presented previously [13], is applied to conduct the present numerical study. The numerical model accounts for electrochemical and transport phenomena in all nine regions of a PEFC, including the gas channels, the diffusion and catalyst layers, and the current collectors on both the anode and cathode sides, and the membrane. Conservation equations of mass, momentum, chemical species, proton and electron charge, as presented in Table 1, are numerically solved, with appropriate account of the electrochemical kinetics.

The mass and momentum equations are numerically solved to obtain the flow-field. Superficial velocities are used in these equations in order to automatically ensure mass flux continuity at the interface between the porous GDL and non-porous gas channel. The source terms in the momentum equations are implemented based on Darcy's law, representing an extra drag force proportional to fluid viscosity and velocity, and inversely proportional to the permeability of a porous medium.

The species concentration equations, including hydrogen and water at the anode side, and oxygen and water at the cathode side, are solved to obtain reactant and product distributions. The source/sink terms in these equations are implemented based on the electrochemical kinetics. In the water transport equation, inside the membrane/electrode assembly (MEA), an extra source term is added to account for the electro-osmotic drag.

A proton conservation equation is solved inside the MEA, ensuring accurate account of the ionic resistance in this region. It has been found that the ionic resistance in the anode and cathode catalyst layers is comparable to that in the membrane, indicating that the catalyst layers cannot be neglected in PEFC modelling [12].

An additional electron transport equation is numerically solved in the catalyst and gas diffusion layers, and in the current collector in the PEFC model of Meng and Wang [13]. Because of the inclusion of the electron transport equation, the current density boundary condition can now be directly implemented on the outer surface of the bipolar plate on the cathode side. This new capability enables, for the first time, the present numerical study of the effects of electron transport on current distribution and cell performance under the prescribed current density boundary condition.

Details of the PEFC model and its numerical implementation were given in [13] and, therefore, will not be repeated here.

Table 1 Conservation equations.

| | Conservation equations | | Source terms |
|---|---|---|---|
| Mass | $\nabla \cdot (\rho \vec{u}) = 0$ | (1) | |
| Momentum | $\frac{1}{\varepsilon^2}\nabla \cdot (\rho \vec{u}\vec{u}) = -\nabla p + \nabla \cdot \tau + S_u$ | (2) | in diffusion and catalyst layers: $S_u = -\frac{\mu}{K}\vec{u}$ |
| Species concentration | $\nabla \cdot (\vec{u}c_i) = \nabla \cdot (D_i^{eff}\nabla c_i) + S_i$ | (3) | in catalyst layers: $S_i = -\frac{s_i j}{nF}$ except water; $S_i = -\nabla \cdot \left(\frac{n_d}{F} i_e\right) - \frac{s_i j}{nF}$ for water in MEA |
| Proton | $\nabla \cdot (\kappa^{eff}\nabla \phi_e) + S_\phi = 0$ | (4) | in catalyst layers: $S_\phi = j$ |
| Electron | $\nabla \cdot (\sigma^{eff}\nabla \phi_s) + S_\phi = 0$ | (5) | in catalyst layers: $S_\phi = -j$ |

Electrochemical reactions: $\sum_i s_i M_i = ne^-$ where $M_i \equiv$ chemical formula of species i; $s_i \equiv$ stoichiometry coefficient; $n \equiv$ number of electrons transfered

Hydrogen oxidation reaction at anode side: $H_2 - 2H^+ = 2e^-$ (6)

Oxygen reduction reaction at cathode side: $2H_2O - O_2 - 4H^+ = 4e^-$ (7)

## 3 Results and Discussion

### 3.1 Theoretical Analysis

Figure 1 shows the schematic of a PEFC with a straight gas channel. The typical plate thickness is 1,500 μm, the half width 1,000 μm, and the along-channel length 100,000 μm. The electronic conductivity is 20,000 S $m^{-1}$ for graphite-based materials (metals are more than ten times higher, as discussed later in the parametric study). The typical electronic resistance in the through-plane direction is derived as

$$R_1 = \frac{t}{\sigma} = \frac{1{,}500\ \mu m}{20{,}000\ S\,m^{-1}} = 0.75\ m\Omega\,cm^2 \quad (8)$$

The electronic resistance in the lateral direction in the land is

$$R_2 = \frac{w}{\sigma} = \frac{1{,}000\ \mu m}{20{,}000\ S\,m^{-1}} = 0.5\ m\Omega\,cm^2 \quad (9)$$

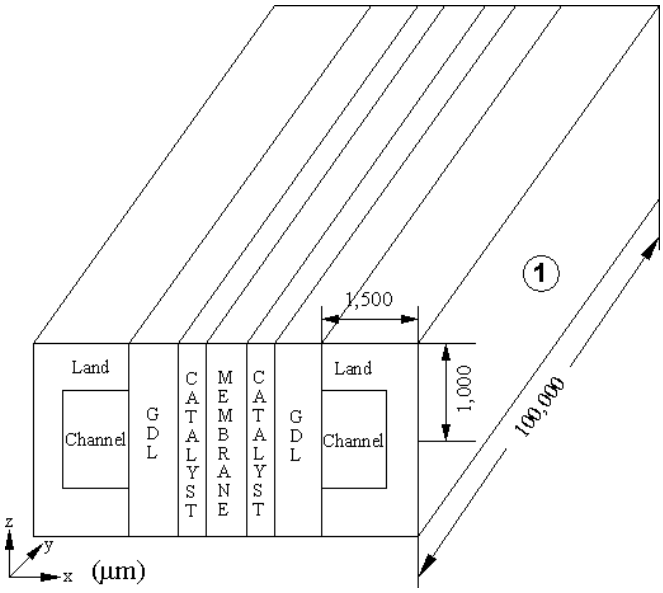


Fig. 1 Geometry of a single straight-channel polymer electrolyte fuel cell.

The electronic resistance in the along-channel direction is

$$R_3 = \frac{L}{\sigma} = \frac{100{,}000\ \mu m}{20{,}000\ S\,m^{-1}} = 50\ m\Omega\,cm^2 \quad (10)$$

The electronic resistance in the along-channel direction is much larger than in the other two directions, which will significantly affect current flow in the current collector plate, and current and electric potential distributions in a PEFC, as discussed in the next section.

It should be noted that the basic parameter affecting cell performance in a PEFC is the potential variation, which is proportional to both current density and electronic resistance. Since current densities along the three directions in the land could differ significantly in a PEFC, the electronic resistances are not directly comparable.

### 3.2 Numerical Results and Discussion

The effects of the electronic resistance in the current collector plate on current distribution and cell performance were numerically investigated, based on a single straight-channel PEFC with co-flow of anode and cathode gases, as shown in Figure 1. The cell geometry is presented in Table 2. A careful grid independence study has been conducted to ensure accurate numerical results. In the present numerical calculations, a total of 316,800 computational cells were found to be sufficient to provide grid-independent results.

Table 2 Cell geometry.

| Fuel cell geometry / mm | | |
|---|---|---|
| Cell length | | 100.00 |
| Gas channel | Depth | 1.000 |
| | Width | 1.000 |
| Layer thickness | Diffusion | 0.300 |
| | Catalyst | 0.010 |
| | Membrane | 0.025 |
| Land width | | 0.500 |
| Land thickness outside gas channel | | 0.500 |
| Computational cell numbers | | ~310,000 |

Table 3 Electrochemical and transport parameters.

| | |
|---|---|
| Anode total exchange current density, $aj_0$ / A m$^{-3}$ | 1.0E+9 |
| Cathode total exchange current density, $aj_0$ / A m$^{-3}$ | 1.0E+4 |
| Reference hydrogen concentration, $C_{H2}$ / mol m$^{-3}$ | 40 |
| Reference oxygen concentration, $C_{O2}$ / mol m$^{-3}$ | 40 |
| Anode transfer coefficients | $\alpha_a = \alpha_c = 1$ |
| Cathode transfer coefficient | $\alpha_c = 1$ |
| Faraday constant, $F$ | 96,487 |
| Porosity of diffusion layer | 0.6 |
| Porosity of catalyst layer | 0.112 |
| Volume fraction of ionomer in catalyst layer | 0.4 |
| Permeability of the diffusion layer / m$^2$ | 1.0E-15 |
| Equivalent weight of ionomer / kg mol$^{-1}$ | 1.1 |
| Dry membrane density / kg m$^{-3}$ | 1,980 |
| Universal gas constant / J mol$^{-1}$ K$^{-1}$ | 8.314 |
| Electronic conductivity in current collector / S m$^{-1}$ | 20,000 |
| Effective electronic conductivity in GDL / S m$^{-1}$ | 500 |

The fuel cell was operated at 80 °C and 2 atm with fully-humidified hydrogen and air fed into the anode and cathode inlets, respectively. The stoichiometry value on both sides was set at 2.5, based on the actual current density applied to the cell. In the present numerical study, no contact resistance between two mating materials in the PEFC was considered. Therefore, the calculated cell performance is better than could be expected for real-world PEFC operation, i.e., at 0.8 A cm$^{-2}$, the calculated cell voltage is 0.689 V. It should be emphasized that the contact resistance has a significant effect on cell performance, as discussed in detail by Meng and Wang [13]. The electrochemical and transport parameters are listed in Table 3.

Figure 2 presents current density profiles in the along-channel direction. Two boundary conditions were applied on the outer surface on the cathode current collector plate (surface 1 in Figure 1): constant cell voltage and constant current

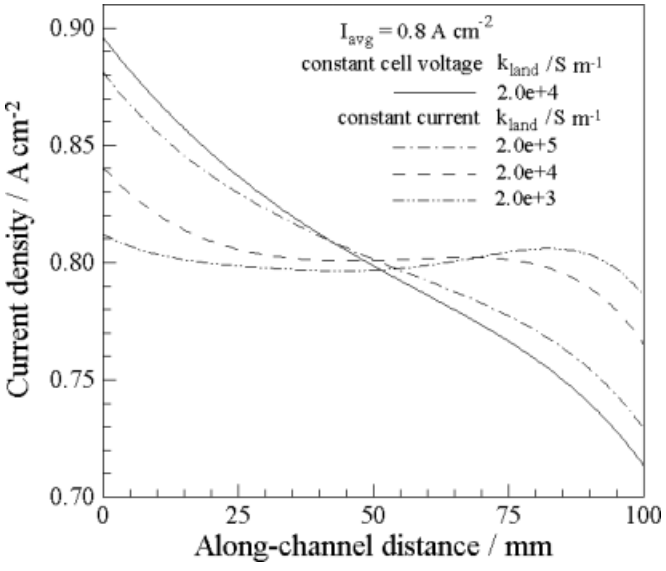


Fig. 2 Current density profiles in the along-channel direction using two different boundary conditions.

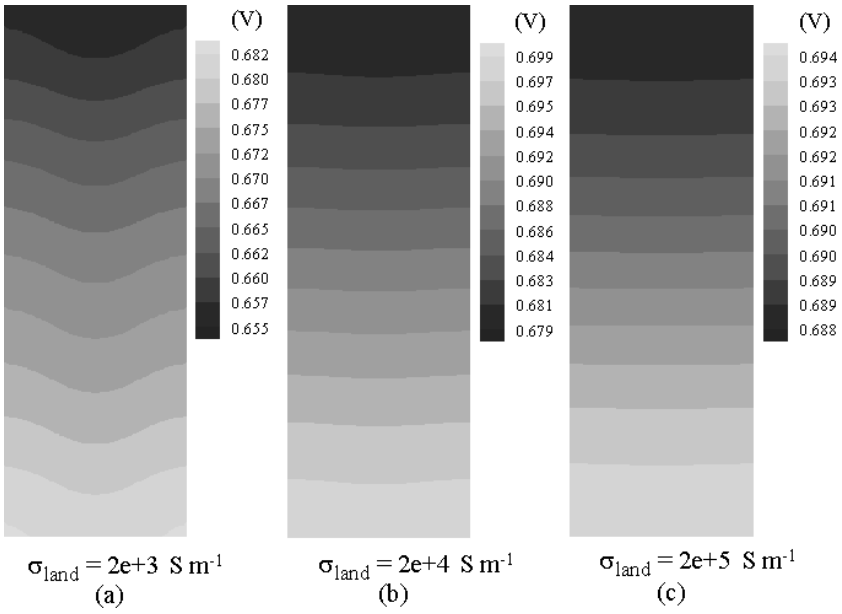


Fig. 3 Electronic phase potential (V) distributions on the base surface of the cathode current collector plate.

density, while a constant electrical potential of zero was implemented on its anode counterpart. At a current collector plate electronic conductivity of 20,000 S $m^{-1}$ (typical value for graphite materials), the numerical calculation with a constant current density of 0.8 A $cm^{-2}$, specified on the cathode boundary, results in an average cell voltage of 0.689 V, while a constant cell voltage of 0.689 V on the boundary produces an average current density of 0.8 A $cm^{-2}$. The same phenomenon has been verified at other operating conditions with the average current density ranging from 0.2 to 1.6 A $cm^{-2}$ and the average cell voltage from 0.8 to 0.4 V. Therefore, the results under the two different boundary conditions will produce an identical cell polarization curve, but the current density variations in the along-channel direction under the two boundary conditions are vastly different. Under the constant current boundary condition the current density is flatter, as shown in Figure 2. The present results have a profound impact on the way all numerical PEFC models should be validated. Model validation based on the polarization curve alone is insufficient, and the detailed current density distribution in the along-channel direction is, at least, required to provide more confidence in PEFC models.

The reason the current distributions under the two boundary conditions are different is related to the large electronic resistance, 50 mΩ $cm^2$, in the along-channel direction in the current collector plate. With the existence of this large electronic resistance, current flow in the along-channel direction will cause a significant ohmic drop in the plate on the cathode side. At the boundary condition with a constant current density of 0.8 A $cm^{-2}$ on the cathode base surface, the electronic phase potential difference between the inlet and the outlet amounts to 20 mV, as seen in Figure 3b. This local difference in electronic phase potential alters the local surface over-potential for the oxygen reduction reaction (ORR) and hence the local current density distribution. Figure 4 presents the electronic and electrolyte phase potential profiles in the through-plane direction across the MEA, directly under the middle of the gas channel. The difference in the cathode over-potentials between the inlet (at $y/y_0 = 0.1$ from the inlet end) and the outlet (at $y/y_0 = 0.9$) is close to 20 mV, which comes almost entirely from the difference in the electronic phase potential in the cathode current collector plate. The over-potential difference of 20 mV has a significant effect on the reaction current since according to the Tafel slope of the ORR, an over-potential difference of ~60 mV gives rise to an order of magnitude change in current density. Under the current density boundary condition, although the lower oxygen concentration at the cell outlet would cause a decrease in reaction current, the higher surface over-potential in the cathode catalyst layer largely compensates for that decrease, resulting in a flatter current profile in the along-channel direction, as shown in Figure 2.

The electronic resistance in the current collector plate varies significantly if different materials are used. For example, the electronic conductivities of metals are of the order of $10^5$ S $m^{-1}$, which is ten times that of graphite. Using metals to manufacture the current collector plate enhances electron transport in the along-channel direction and, therefore, reduces the electronic phase potential difference between the inlet and the outlet. Thus, a parametric study was conducted to verify this by changing the electronic conductivity of the current collector plate. As shown in Figure 2, once the electronic conductivity has been increased

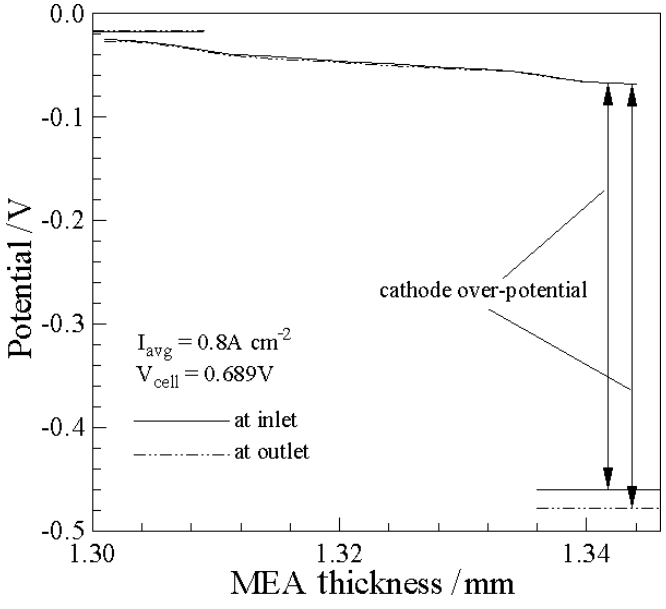


Fig. 4 Electronic and electrolyte phase potential profiles through the MEA under the gas channel using the constant current density boundary condition.

  

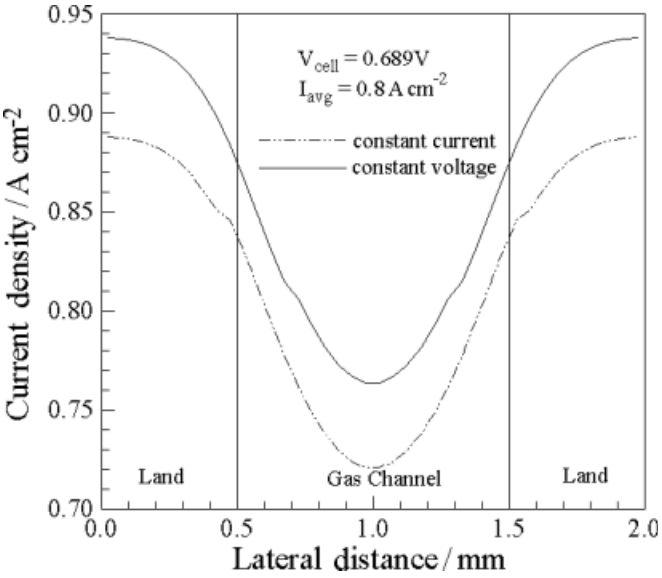


Fig. 5 Current density profiles inside the membrane in the lateral direction near the inlet using two different boundary conditions.

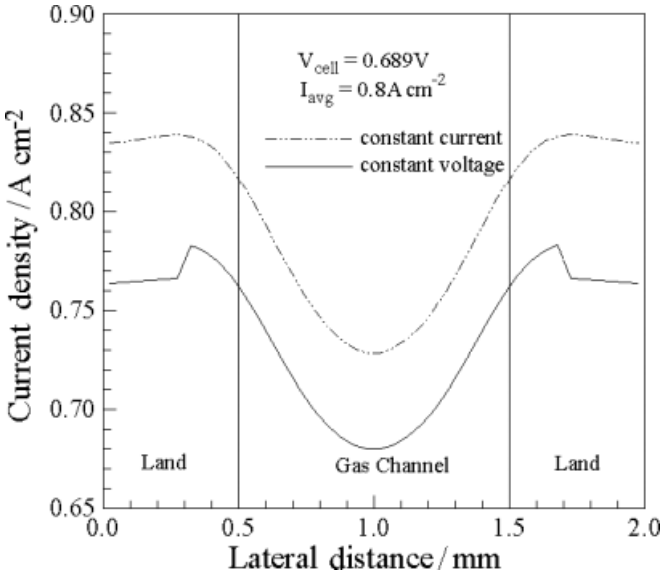


Fig. 6 Current density profiles inside the membrane in the lateral direction near the outlet under two different boundary conditions.

ten times to 200,000 S m$^{-1}$, the current distribution under the constant current density boundary condition of 0.8 A cm$^{-2}$ approaches that seen under the constant cell voltage boundary condition. In this case, the local difference in electronic phase potential on the surface of the cathode current collector plate decreases to around 6 mV, as shown in Figure 3c. By reducing the electronic conductivity of the bipolar plate to 2,000 S m$^{-1}$, the local difference in electronic phase potential in the cathode bipolar plate between the inlet and the outlet increases to more than 27 mV, resulting in an even flatter current profile in the along-channel direction, as shown in Figures 3a and 2, respectively. Figure 2 clearly points to the possibility of controlling the current distribution in PEFCs by matching with bipolar plates of the appropriate electronic conductivity.

The electronic phase potential variation in the lateral direction (the z-coordinate direction) in the bipolar plate is negligible because the electronic resistance is very small, i.e., 0.5 mΩ cm$^2$. Figure 5 compares current density profiles inside the membrane in the lateral direction near the inlet ($y/y_0$ = 0.1) under the two different boundary conditions. The profiles are similar, except that the magnitude is shifted downwards under the current density boundary condition because of the higher local electronic phase potential in the current collector plate, i.e., 0.699 V *vs.* 0.689 V. At the inlet end, since the oxygen concentration is the same, the difference between the two curves is caused entirely by the difference in the local surface over-potential.

At the outlet end ($y/y_0$ = 0.9), the situation is reversed. As shown in Figure 6, the entire curve under the constant current density boundary condition now shifts upwards. The difference between the two curves is caused not only by the larger over-potential, but also by the higher oxygen concentration under the constant current density boundary condition. The surface over-potential in the cathode catalyst layer is larger at the outlet under the current density boundary condition because the electronic phase potential is lower in the current collector plate, i.e., 0.679 V *vs.* 0.689 V, while the oxygen concentration is higher because the current density at the inlet is lower and less oxygen is consumed.

The current density variation in the lateral direction is determined by both electronic resistance and oxygen transport [13]. This conclusion is true at both constant current density and constant cell voltage boundary conditions. Figure 7 displays the cross-sectional distributions of the electronic potential in the GDL at $y/y_0$ = 0.5 on both the anode and cathode sides under the constant current density boundary

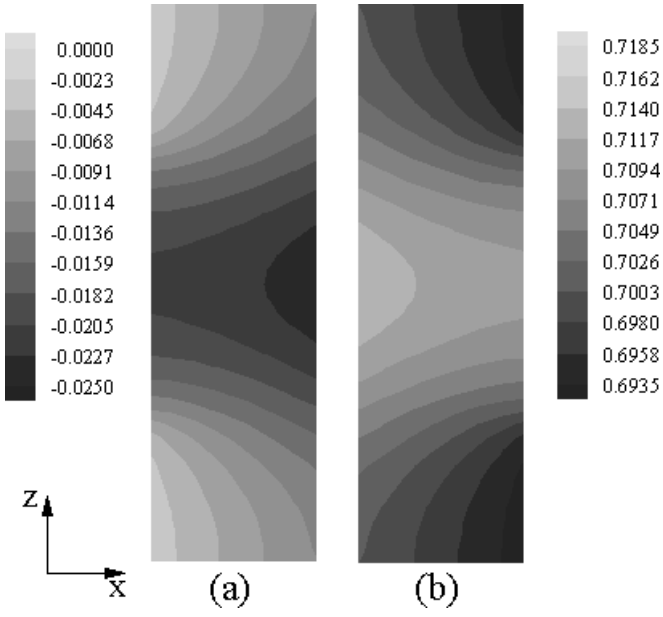


Fig. 7 Distribution of the electronic phase potential (V) in the GDL on (a) the anode and (b) the cathode side, using the constant current density boundary condition.

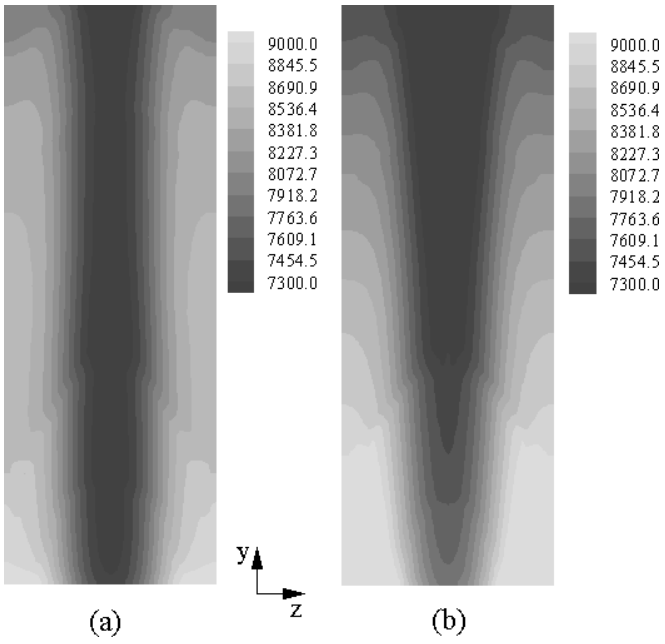


Fig. 8 Current distribution (A $m^{-2}$) in the middle of the membrane under (a) constant current density, and (b) constant cell voltage boundary conditions.

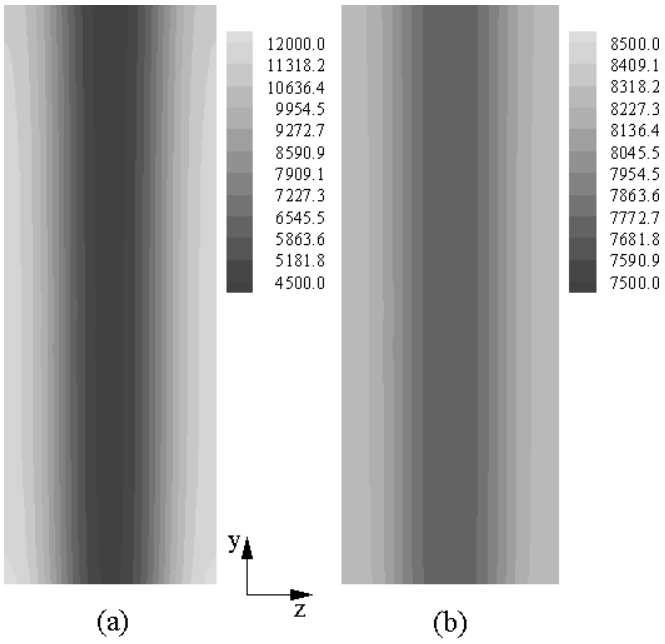


Fig. 10 Current distribution (A $m^{-2}$) in the bipolar plate on (a) the anode and (b) the cathode side, under the constant current density boundary condition.

condition. The lowest electronic potential was shown in the anode GDL and the highest value in the cathode GDL under the middle of the gas channel, since the travelling distance, for electrons to reach the current conducting land, is longest from there, resulting in the largest electronic resistance.

Current distributions in the middle of the membrane, under the two different boundary conditions, are compared in Figure 8. The effects of the two boundary conditions are clearly illustrated.

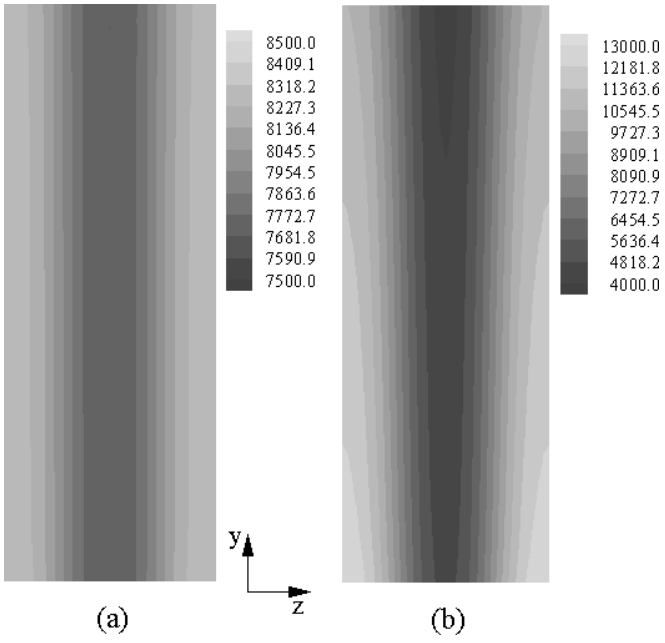


Fig. 9 Current distribution (A $m^{-2}$) in the cathode bipolar plate under (a) constant current density, and (b) constant cell voltage boundary conditions.

The current distribution in the current collector plate can be obtained since it is where the electron transport equation is solved. Figure 9 presents current distributions inside the plate, outside the cathode gas channel, under both constant current density and constant cell voltage boundary condi-

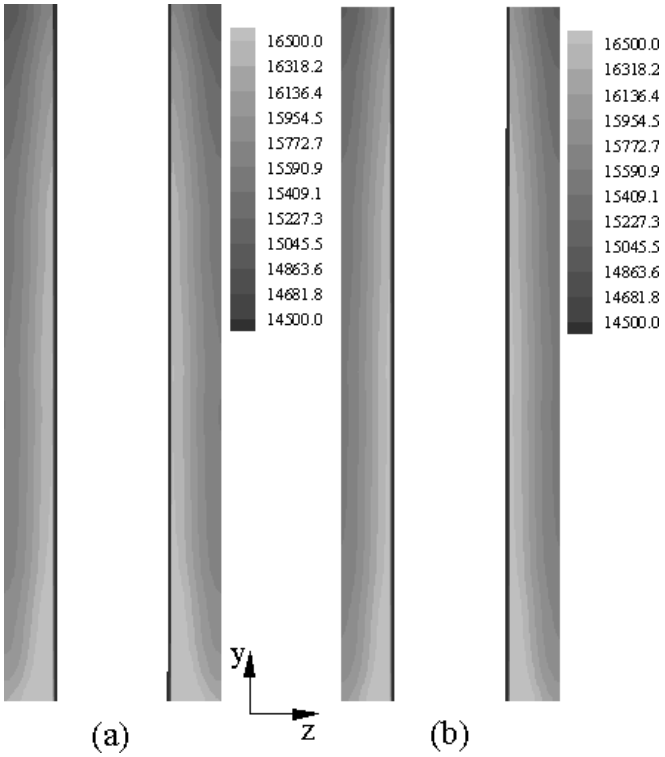


Fig. 11 Current distribution (A $m^{-2}$) inside the lands on (a) the anode and (b) the cathode side, under the constant current density boundary condition.

  

tions. As expected, the current distribution is more uniform at the constant current density boundary condition. However, the current density is not a constant inside the plate even though it is defined as a constant on the outer surface. Because of the existence of the gas channel, electrons have to be transferred through the two lands, resulting in significant lateral electron transport in the bipolar plate outside the gas channel. This phenomenon is clearly illustrated in Figure 9b, under the constant cell voltage boundary condition. In this case, the current density difference in the lateral direction can be as high as 7,000 A $m^{-2}$ or 0.7 A $cm^{-2}$. This difference is strongly affected by the land and channel widths. Decreasing the land width and/or increasing the channel width will further enlarge the current density non-uniformity.

Figure 10 compares current distributions in the bipolar plate outside the gas channel on both the anode and cathode sides, under the constant current density boundary condition. The current distribution is more uniform in the plate on the cathode side because the cathode plate is under the constant current density boundary condition, whereas the anode plate is at a constant set potential (i.e., at 0 V). Figure 11 presents the current distributions inside the lands on both the anode and cathode sides. The current distributions are almost the same on both sides, affected entirely by the electron production/consumption in both the anode and cathode catalyst layers. Therefore, the difference in the current distributions on the anode and cathode sides, Figure 10, mainly occurs in the base of the bipolar plate.

## 4 Conclusion

A three-dimensional, single-phase, isothermal numerical model of a polymer electrolyte fuel cell has been used to study the effects of electron transport on the current distribution and cell performance of a PEFC under the prescribed current density boundary condition and real stoichiometry control.

Because of the geometrical features of the PEFC, the electronic resistance in the along-channel direction in the current collector plate is much larger than the resistances in the other two directions, i.e., 50 mΩ $cm^2$ *vs.* 0.5 mΩ $cm^2$, which significantly affects current and cell voltage distributions in the PEFC. Results obtained using two different boundary conditions have been compared, constant cell voltage and constant current density, defined on the base surface of the cathode current collector plate. Identical polarization curves are obtained, but the current density profiles in the along-channel direction are very different; the profile in the case of the constant current density boundary condition is flatter. This mainly results from the fact that the large electronic resistance in the along-channel direction gives rise to a significant difference in the electronic phase potential in the bipolar plate, under the constant current density boundary condition. Increasing the electronic conductivity of the current collector plate, i.e., using metals, the difference in the current density profiles under the two boundary conditions would diminish. The present results further support the view that numerical validation of a PEFC model based on the cell polarization curve alone is insufficient, and that a detailed current distribution in the along-channel direction is essential.

The current density profiles in the lateral direction, governed by both electronic resistance and oxygen supply, show the same trend under the two different boundary conditions, except the entire curve is shifted downwards at the inlet and upwards at the outlet under the constant current density boundary condition.

The local current density is not constant inside the bipolar plate under either boundary condition, even though the electronic conductivity is 20,000 S $m^{-1}$. Under the constant cell voltage boundary condition, the current distribution in the plate is caused solely by electron transport in the lateral direction, while under the constant current density boundary condition, it results from electron transport in both the lateral and along-channel directions, and becomes more uniform.

## Acknowledgements

Funding for this work from the DOE ultra-clean fuel program under cooperative agreement No. DE-FC26-01NT41098 is acknowledged. Support from Toyota Motor Corporation and General Motors is also gratefully acknowledged.

## List of Symbols

| | |
|---|---|
| $c$ | Molar concentration / mol $m^{-3}$ |
| $D$ | Mass diffusivity / $m^2$ $s^{-1}$ |
| $F$ | Faraday constant / 96,487 C $mol^{-1}$ |
| $j$ | Transfer current density / A $m^{-3}$ |
| $K$ | Permeability / $m^2$ |
| $n$ | Number of electrons in electrochemical reaction |
| $n_d$ | Electroosmotic drag coefficient |
| $p$ | Pressure / Pa |
| $s$ | Stoichiometry coefficient in electrochemical reaction |
| $S$ | Source term in transport equation |
| $u$ | Fluid velocity and superficial velocity in porous medium / m $s^{-1}$ |

*Greek*

| | |
|---|---|
| $\Phi$ | Phase potential / V |
| $\mu$ | Viscosity / kg $m^{-1}$ $s^{-1}$ |
| $\rho$ | Density / kg $m^{-3}$ |
| $\kappa$ | Proton conductivity / S $m^{-1}$ |
| $\sigma$ | Electronic conductivity / S $m^{-1}$ |

*Superscripts*

| | |
|---|---|
| eff | Effective value in a porous medium |

  

*Subscripts*

e Electrolyte
i Species index
s Electron

## References

[1] V. Gurau, H. Liu, S. Kakac, *AIChE Journal* **1998**, *44*, 2410.
[2] J. S. Yi, T. V. Nguyen, *Journal of the Electrochemical Society* **1998**, *145*, 1149.
[3] J. S. Yi, T. V. Nguyen, *Journal of the Electrochemical Society* **1999**, *146*, 38.
[4] S. Um, C. Y. Wang, K. S. Chen, *Journal of the Electrochemical Society* **2000**, *147*, 4485.
[5] S. Um, C. Y. Wang, *Journal of Power Sources* **2004**, *125*, 40.
[6] S. Dutta, S. Shimpalee, J. W. Van Zee, *Journal of Applied Electrochemistry* **2000**, *30*, 135.
[7] S. Dutta, S. Shimpalee, J. W. Van Zee, *International Journal of Heat and Mass Transfer* **2001**, *44*, 2029.
[8] T. Zhou, H. Liu, *International Journal of Transport Phenomena* **2001**, *3*, 177.
[9] T. Berning, D. M. Liu, N. Djilali, *Journal of Power Sources* **2002**, *106*, 284.
[10] W. K. Lee, S. Shimpalee, J. W. Van Zee, *Journal of The Electrochemical Society* **2003**, *150*, A341.
[11] S. Mazumder, J. V. Cole, *Journal of The Electrochemical Society* **2003**, *150*, A1503.
[12] H. Meng, C. Y. Wang, *Chemical Engineering Science* **2004**, *59*, 3331.
[13] H. Meng, C. Y. Wang, *Journal of the Electrochemical Society* **2004**, *151*, A358.
[14] E. Middelman, W. Kout, B. Vogelaar, J. Lenssen, E. de Wall, *Journal of Power Sources* **2003**, *118*, 44.